# Gastag: A Gas Sensing Paradigm using Graphene-based Tags

Xue Sun[†‡], Jie Xiong[♯], Chao Feng[†‡§], Xiaohui Li[†], Jiayi Zhang[†]

Binghao Li[†], Dingyi Fang[†‡§], Xiaojiang Chen[†‡♮⋄]

[†]Northwest University, [♯]Microsoft Research Asia and University of Massachusetts Amherst
[‡]Shaanxi International Joint Research Centre for the Battery-Free Internet of Things
[§]Xi'an Key Laboratory of Advanced Computing and System Security
[♮]Xi'an Advanced Battery-Free Sensing and Computing Technology International Science and Technology Cooperation Base
[†]{sunxue, zhangjy, libinghao}@stumail.nwu.edu.cn, [♯]jxiong@cs.umass.edu,
[†]Lxiaohuix@163.com, [†]{chaofeng, dyf, xjchen}@nwu.edu.cn

## ABSTRACT

Gas sensing plays a key role in detecting explosive/toxic gases and monitoring environmental pollution. Existing approaches usually require expensive hardware or high maintenance cost, and are thus ill-suited for large-scale long-term deployment. In this paper, we propose Gastag, a gas sensing paradigm based on passive tags. The heart of Gastag design is embedding a small piece of gas-sensitive material to a cheap RFID tag. When gas concentration varies, the conductivity of gas-sensitive materials changes, impacting the impedance of the tag and accordingly the received signal. To increase the sensing sensitivity and gas concentration range capable of sensing, we carefully select multiple materials and synthesize a new material that exhibits high sensitivity and high surface-to-weight ratio. To enable a long working range, we redesigned the tag antenna and carefully determined the location to place the gas-sensitive material in order to achieve impedance matching. Comprehensive experiments demonstrate the effectiveness of the proposed system. Gastag can achieve a median error of 6.7 *ppm* for $CH_4$ concentration measurements, 12.6 *ppm* for $CO_2$ concentration measurements, and 3 *ppm* for *CO* concentration measurements, outperforming a lot of commodity gas sensors on the market. The working range is successfully increased to 8.5 *m*, enabling the coverage of many tags with a single reader, laying the foundation for large-scale deployment.

⋄ Corresponding author.


*ACM MobiCom '24, November 18-22, 2024, Washington D.C., DC, USA*

ACM ISBN 979-8-4007-0489-5/24/09…$15.00
https://doi.org/10.1145/3636534.3649365

## CCS CONCEPTS

• **Hardware** → **Wireless devices**; • **Human-centered computing** → *Ubiquitous and mobile computing*;

## KEYWORDS

Gas Sensing, RFID, Backscatter, Wireless Sensing, Internet of Things (IoT), Graphene Antenna

**ACM Reference Format:**
Xue Sun[†‡], Jie Xiong[♯], Chao Feng[†‡§], Xiaohui Li[†], Jiayi Zhang[†], Binghao Li[†], Dingyi Fang[†‡§], Xiaojiang Chen[†‡♮⋄]. 2024. Gastag: A Gas Sensing Paradigm using, Graphene-based Tags. In *The 30th Annual International Conference on Mobile Computing and Networking (ACM MobiCom '24), September 30-October 4, 2024, Washington D.C., DC, USA.* ACM, New York, NY, USA, 15 pages. https://doi.org/10.1145/3636534.3649365

## 1 INTRODUCTION

Gas sensing plays a pivotal role in a large number of applications, including indoor air quality monitoring [23], hazardous gas detection [5, 6, 47] and precision agriculture [14]. For instance, to maintain high indoor air quality, the concentration of carbon dioxide ($CO_2$) should be kept below 1000 *ppm* (0.1 % in the air) [63]. Once the $CO_2$ concentration

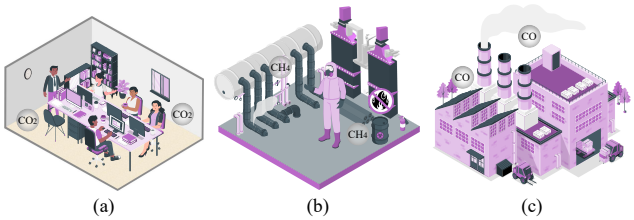


**Figure 1: Example applications of Gastag: (a) Monitoring $CO_2$ in an office; (b) Detecting $CH_4$ leakage in a gas plant; (c) Monitoring $CO$ emission in a factory.**

exceeds this level, it can cause symptoms including discomfort, headache, and mental fatigue [1]. Another example is methane ($CH_4$), which is the primary component of natural gas and is widely used in heating and electricity generation. Methane gas is very dangerous and methane leakage can cause severe incidents. From 2010 to 2021, a total of 2600 gas-related incidents were reported in the United States. Among these incidents, 328 cases resulted in explosions, causing 122 deaths [41]. In developing countries, gas leakage-caused explosions result in over a hundred deaths each year [46].

Gas detection papers/tubes are widely used for gas detection. They can report the existence of a gas but not the more important concentration information. Also, they are usually designed for a single use and are not suitable for long-term monitoring. Existing methods for long-term gas monitoring are mainly based on gas sensors [9]. These sensors are usually battery-powered and have their own shortcomings such as requiring calibration (semiconductor-based [38]), short operational lifetime (electrochemical-based [58]) and expensive (Non-Dispersive Infrared (NDIR)-based [9] and Photoionization detector (PID)-based [22]). For large-scale deployment, these sensors incur high cost and/or high maintenance burden (e.g., battery replacement), rendering them ill-suited for long-term gas monitoring.

Inspired by recent progress on wireless sensing, RFID technologies are actively explored for sensing purposes [12, 15, 48, 52, 55, 61]. The unique advantage of exploiting RFID tags for sensing is that the tags are extremely cheap (the price can be lower than 10 cents) and small in size, making them ideal for large-scale deployment. The basic idea of RFID sensing is that RFID signals are reflected by target motion (e.g., human gesture) and we can extract the motion information by analyzing the signal variations. However, this method can not be applied for gas sensing. This is because compared to the large signal variation caused by target motion, the effect of gas concentration change on signal propagation is extremely small and the induced signal variation is too small to be detected.

Some other works further propose to place RFID tags very close (e.g., with a distance smaller than 2 $cm$) to the sensing target so that the impedance of the tag can be influenced by the target. Different from conventional RFID sensing which influences the signal propagation path, this method captures the influence of the target on the transceivers for sensing. This method has been successfully used to sense the liquid type [55, 61]. However, it is still far from being effective for gas sensing because the amount of impedance change caused by gas concentration change in the air is orders of magnitude smaller than that caused by liquids.

Therefore, although cheap RFID tags are ideal for large-scale deployment, it is challenging to use them for gas sensing. In this paper, we propose a new sensing paradigm based on cheap RFID tags for gas sensing, as shown in Fig. 1. The key idea is to replace a small part of the tag antenna with gas-sensitive material to significantly increase the effect of gas change on the tag and eventually create a large enough signal variation that can be utilized for sensing. Specifically, the gas concentration change can cause the chemical properties of the gas-sensitive material to vary, causing variations of the received signal at the RFID reader. We can thus exploit this signal variation for gas sensing such as concentration measurements. Although promising, we face several challenges before we can turn this idea into a working system.

- To make sure the RFID tag can still communicate with the reader, we can only replace a small part of the tag antenna with the gas-sensitive material. However, with just a small piece of gas-sensitive material, the amount of signal variation caused by gas change is also extremely small, making fine-grained gas sensing challenging. Furthermore, most materials are only sensitive to the gas concentration change in a small range. It is challenging to use a small piece of material to realize fine-grained gas sensing in a large gas concentration range.
- The second challenge is that although gas concentration change can affect the property of the gas-sensitive material and eventually the signal received at the RFID reader, the relationship between the gas concentration and the signal variation is complicated and unknown. Modeling the mathematical relationship without any training or machine learning is challenging.
- Although we replaced just a small part of the tag antenna with gas-sensitive material, we still observed a sharp drop in the communication distance between RFID reader and RFID tags. This small range severely restricts the practicality and adoption of the proposed system for large-scale deployment.
- While the gas concentration can cause signal variations, the signal variations are also affected by other factors such as reader-tag distance/orientation. It is not practical to place the reader and tag always at a fixed

distance and orientation for sensing and it is thus critical to make the proposed system distance-independent and orientation-independent.

To address the first challenge, among those commonly used materials for gas sensing (e.g., nanocomposite, graphene and polymer), we select the one that is most sensitive to the target gas. For example, for $CH_4$, we select polyaniline (PANI) which is a polymer, and for $CO_2$, we select carbon nanotubes (CNTs), which belong to the graphene family. Although sensitive, the workable concentration range for these materials is still limited. Take PANI as an example. The concentration range of $CH_4$ the PANI material is able to sense is between 0-100 $ppm$, far smaller than the targeted range (0-1000 $ppm$) for practical use. Note that the concentration range is mainly determined by the maximum amount of gas a unit weight of material can absorb. To increase the workable concentration range, we thus need to increase the surface area of the sensing material. We find that reduced Graphene Oxide (rGO) is an outstanding candidate with an extremely large surface-to-weight ratio. We therefore synthesize rGO with the gas-sensitive material to form a new synthetic material (e.g., rGO-PANI for $CH_4$ sensing) which exhibits fine sensitivity and at the same time can work in a much larger concentration range. Another exciting property of the new material is that it exhibits a rapid rate of gas adsorption and desorption, making it suitable for real-time monitoring (fast adsorption) and for quick reuse (fast desorption).

To address the second challenge, we dig deeply to understand the relationship between signal variation and gas concentration change. Specifically, the gas concentration change affects the gas material's properties, leading to the impedance change of the tag antenna. This impedance change eventually causes signal variations at the receiver. We mathematically model the relationship to quantify the effect of gas concentration change on signal variations.

To address the third challenge which is the much smaller working distance after the sensing material replaces the original antenna part, we investigate the key factors affecting the reader-tag working distance. We find that impedance mismatch between the tag antenna and tag IC is the key reason causing the decreased distance. We notice that the gas material position (i.e., where the antenna part is replaced) indeed influences the impedance. We therefore establish an equivalent circuit model to analyze the relationship between material position and the impedance value. We further find that although the material placement position affects the impedance, just tuning the material position can not achieve impedance matching. We therefore involve the antenna shape into the loop to design both antenna shape and material position to achieve full impedance matching. This approach can significantly increase the working distance from 0.15 $m$ to 8.5 $m$.

To address the last challenge, i.e., reader-tag distance dependency, we adopt a second tag without any modification as a reference to cancel the effect of distance and other interference. We designed and fabricated Gastag tags for our experiment. The cost of the tag is below 50 cents. We conducted extensive field experiments with a commercial Impinj R420 reader serving as the transceiver. Comprehensive experiments in three typical indoor environments demonstrate that Gastag can achieve accurate, long-range, and robust gas sensing. To summarize, this paper makes the following contributions:

- We present Gastag, a new gas sensing paradigm based on cheap passive RFID tags. We combine several elements of different disciplines, more specifically, material science, RFID tag design and wireless sensing to realize an end-to-end long-range fine-grained gas sensing system using cheap RFID tags for the first time.
- We propose novel designs spanning across hardware and software to address various challenges including limited concentration range, short distance, and distance-dependency. We believe the proposed designs can inspire follow-up research on this exciting area.
- We validated the effectiveness of Gastag with real-world environments. Experiment results show that the sensing range is increased from 0.15 $m$ to 8.5 $m$. Gastag can achieve a median error of 6.7 $ppm$ for $CH_4$, 12.6 $ppm$ for $CO_2$ and 3 $ppm$ for $CO$ concentration measurements in large concentration ranges. The accuracy of Gastag outperforms a large range of commodity gas sensors on the market.

## 2 BACKGROUND ON RFID SYSTEM

A passive RFID system typically consists of a reader and several battery-less passive tags. For communication, the reader transmits periodic continuous wave (CW) signals and the passive tag activates itself by harvesting energy from the CW signal and modulates its data on the backscattered signals using on-off keying, as shown in Fig. 2. We next introduce two important parameters of RFID tags related to our system design.

**Tag Phase.** The phase reading $\theta$ reported by the RFID reader can be expressed as [44]:

$$\theta = (\frac{2\pi}{\lambda} * 2d + \theta_{pol} + \theta_{tag}) \bmod 2\pi, \quad (1)$$

where $\lambda$ is the wavelength of the carrier frequency and $d$ denotes the distance between the reader antenna and tag. $\theta_{pol}$ is the polarization offset induced by the difference of polarization directions between the reader antenna and tag. $\theta_{tag}$ is the phase variation caused by a change in the tag's impedance,

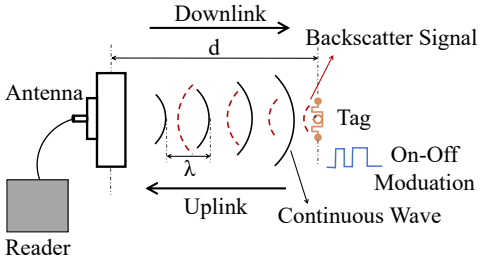


**Figure 2: Operation of an RFID reader and a tag.**

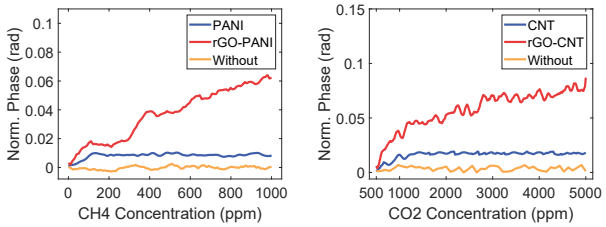


(a) CH4 (b) CO2

**Figure 3: Phase variations when increasing the gas concentration.**

and it can be expressed as $\theta_{tag} = arg(\frac{1}{Z_a+Z_c(off)} - \frac{1}{Z_a+Z_c(on)})$ [4]. $Z_a$ is the antenna impedance, $Z_c(off)$ and $Z_c(on)$ respectively denote the chip impedance $Z_c$ in two states. Since $Z_{off}$ is usually very large [4], $\theta_{tag}$ can thus be expressed as:

$$\theta_{tag} = arg(-\frac{1}{Z_a + Z_c(on)}). \quad (2)$$

As shown in the above equation, the phase reading is mainly affected by four parameters, i.e., $\lambda$, $d$, $\theta_{pol}$ and $Z_a$. *To use phase information to sense gas concentration, we need to link antenna impedance $Z_a$ with the change of gas concentration.* This is because given a fixed deployment between the tag and reader, $d$ and $\theta_{pol}$ are constants. $\lambda$ is also a constant as gas concentration change has a negligible effect on it.

**Tag Chip Threshold Power.** To activate the passive tag, the harvested power $P_c$ should be larger than the minimum power $P_{threshold}$ required to power up the chip. Generally, $P_c$ can be expressed as [3]:

$$P_c = (1 - |\Gamma|^2) G_{tag} G_t P_t \rho^2 (\frac{\lambda}{4\pi d})^2, \quad (3)$$

where $P_t$ is the transmission power, $G_t$ is the gain of the reader antenna, $G_{tag}$ is the gain of the tag antenna, $\rho$ is the polarization loss factor and $\Gamma = \frac{Z_c - (Z_a)^*}{Z_c + (Z_a)}$. Thus, *to increase the working distance between reader and tag, we can increase $G_{tag}$ and $P_t$, or achieve impedance matching with $\Gamma = 0$.*

## 3 DESIGN OF GASTAG

In this section, we first introduce how Gastag synthesizes new gas-sensitive material to sense the gas concentration changes. Then, we explain how Gastag embeds the gas-sensitive materials into a tag and modifies the tag shape to enable a long working range.

### 3.1 Gas-sensitive Material Preparation

*3.1.1 Choices of Gas-sensitive Materials.* To enable low-cost, accurate, and practical gas sensing, the gas-sensitive material should meet the following requirements: (i) Easy to fabricate; (ii) Fast response to gas changes; and (iii) Work under room temperature (i.e., does not require a very high temperature to work). Among those commonly used materials for gas sensing (e.g., nanocomposite, graphene and polymer), we select the one that is most sensitive to the target gas. For example, for $CH_4$, we select polyaniline (PANI) which is a polymer, and for $CO_2$, we select carbon nanotubes (CNTs), which belong to the graphene family.

We first characterize the gas-sensing performance of PANI. We embed this material into an RFID tag by replacing a part of the antenna with a length of 4 *mm* at a distance of 3 *mm* from the chip with the gas-sensitive material as shown in Fig. 6. We conduct a benchmark experiment by varying the concentration of $CH_4$ from 0 to 1000 *ppm* and the concentration of $CO_2$ from 500 to 5000 *ppm*. We collect the phase readings of the modified tag and the original tag, respectively. The results are shown in Fig. 3. We can see that without the gas-sensitive material, the phase readings of the original tag do not change with the concentration. With the gas-sensitive material in the tag, we do see the changes. For $CH_4$, the phase increases from 0 to 0.01 *rad* (0.57°) when the concentration is increased from 0 to 100 *ppm*. However, when the concentration is further increased, the phase does not change much. These results imply that although the gas-sensitive material is effective, it has a very small working concentration range.

Generally, when the gas-sensitive material is exposed to a specific gas, a certain amount of gas molecules will be adsorbed to the material. This adsorption causes a redistribution of electrons within the material molecule, leading to a change in its electrical conductivity [39]. Note that the working concentration range of a gas material is determined by the maximum amount of gas a unit weight of the material can adsorb [40]. With a larger surface-to-weight-ratio (SWR), more gas molecules can be adsorbed. Hence, to make the gas-sensitive material have a large working concentration range, we need to increase the *SWR* of gas-sensitive materials.

*3.1.2 Improving the SWR of Gas-sensitive Materials.* To improve the *SWR*, we propose to synthesize the gas-sensitive materials with the Reduced Graphene Oxide (rGO). rGO has a layered structure that contains many tiny pores. This microporous structure can provide more surfaces and facilitate the diffusion and adsorption of gas, increasing the *SWR* of the material. Thus, by fusing the gas-sensitive material with

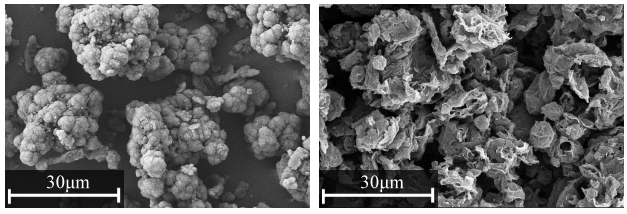


(a) PANI, SWR: 0.3 $m^2/g$ (b) rGO-PANI, SWR: 27 $m^2/g$

**Figure 4: SEM images of gas-sensitive materials.**

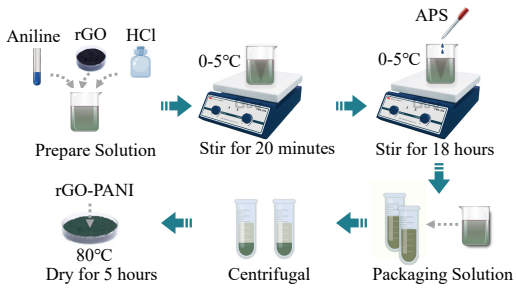


**Figure 5: Process of composing rGO-PANI.**

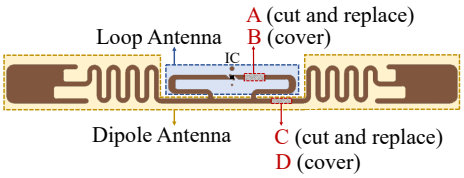


**Figure 6: The basic antenna structure of tag.**

rGO, we can effectively increase the *SWR* of the material. We employ the chemical fusion process [59] to synthesize the new material. The detailed material synthesis process is presented in Fig. 5.

To verify the effectiveness of the synthesized material, we conduct benchmark experiment by varying the concentration of $CH_4$ from 0 to 1000 $ppm$ and collect the phase readings. The result is shown in Fig. 3(a). We can clearly see that the phase readings now continue to increase after 100 $ppm$. The phase increases from 0 to 0.06 $rad$ (3.42°) when the concentration is increased from 0 to 1000 $ppm$.

Finally, we use Scanning Electron Microscopy (SEM) [37] to visualize the material surface morphology. The results are presented in Fig. 4. We utilize a surface area testing instrument [35] to measure the surface area of PANI, which is 0.3 $m^2/g$. Compared to PANI, the structure of rGO-PANI possesses layers and pores, providing a much larger surface area for gas adsorption. The SWR of rGO-PANI is measured as 27 $m^2/g$, 90 times larger than the original material. These results imply that the proposed scheme can effectively increase the *SWR* of the material to enlarge the gas concentration range the material is able to sense.

## 3.2 Tag Antenna Design

In this section, we elaborate on our tag antenna design including: (i) how Gastag embeds the gas-sensitive material to the antenna to achieve accurate sensing; and (ii) how Gastag maximizes the working range of the sensing tag for long-range monitoring.

*3.2.1 The Basic Structure.* Gastag adopts the tag shape design of commercial RFID tags as the basic structure, which is easy to fabricate at a low cost and has a desired omnidirectional radiation pattern. As illustrated in Fig. 6, the antenna has a simple structure, which consists of a loop antenna, a folded dipole antenna, and a chip (IC).

*3.2.2 How to Embed Gas-sensitive Material.* A straightforward way is to make the antenna totally or partially with the gas-sensitive material. However, this design severely degrades the antenna performance, leading to an extremely small working distance between the reader and the tag. Another option is to dope the material on the surface of the tag antenna. However, such a solution presents a poor gas-sensing sensitivity. Ideally, we would like our design to have a high sensitivity and at the same time maintain a reasonably large working distance which is critical for large-scale deployment. To achieve these objectives, we build an equivalent circuit to analyze the relationship between the location of the material and the sensing performance. We take one basic tag structure as an example to illustrate our design. The tag antenna consists of two parts: a loop antenna and a dipole antenna. We adopt two methods to embed the material in each part. Specifically, we cut off a small part of the antenna and replace it with the gas-sensitive material (i.e., Method A and C), or directly cover a small part of the antenna with the material (i.e., Method B and D) as shown in Fig. 6.

Next, we build the equivalent circuit corresponding to each position, as shown in Fig. 7. To calculate the change in the antenna's impedance $Z_a$, we need to calculate the added material's impedance $Z_m$. We utilize the surface impedance model to calculate the material's impedance [31]:

$$Z_m = \sqrt{\frac{j2\pi f \mu_0 \mu_r}{\sigma + j\omega\varepsilon_0}}, \tag{4}$$

where $f$ is the working frequency, $\mu_0$ is the air magnetic permeability and $\mu_r$ is the relative magnetic permeability. The gas-sensing material is non-magnetic material and its $\mu_r$ can be regarded as 1. $\sigma$ is the material conductivity at high frequency and $\varepsilon_0$ is the air permittivity. $\sigma$ can be further expressed as:

$$\sigma = \frac{\sigma_0}{1 + j2\pi f \tau}, \tag{5}$$

here $\sigma_0$ is the material conductivity under direct current (DC). $\tau$ is the relaxation time for free electrons, and $2\pi f \tau << 1$.

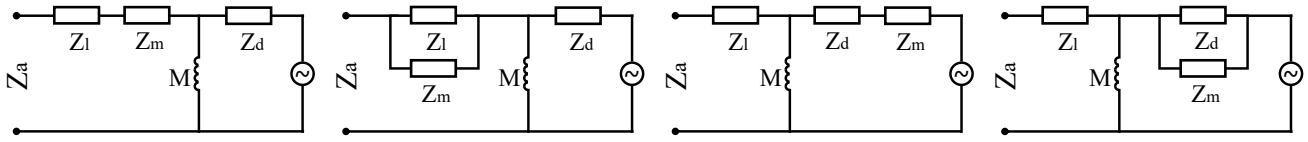


(a) Method A (b) Method B (c) Method C (d) Method D

**Figure 7: Equivalent circuits corresponding to possible material placement locations on the tag.**

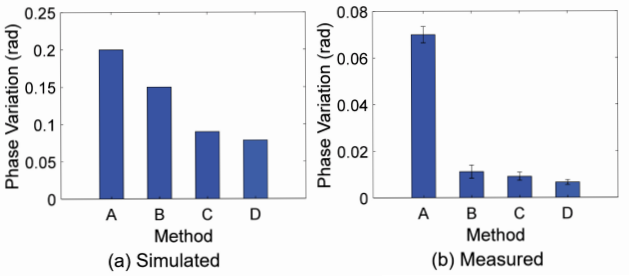


**Figure 8: Phase variation for different methods.**

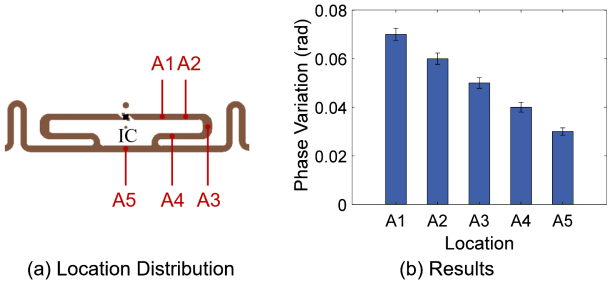


**Figure 9: Estimated phase variation of different cut locations in the loop antenna.**

After obtaining $Z_m$, we move forward to calculate $Z_a$. Specifically, when the loop antenna is cut and replaced with gas-sensitive material, its impedance $Z_l$ is in series with the material's impedance $Z_m$ as shown in Fig. 7(a). $Z_a$ can thus be calculated as $Z_a = Z_l + Z_m + \frac{(\omega M)^2}{Z_d}$, where $Z_d$ is the dipole antenna's impedance, and $M$ is the mutual inductance between the loop antenna and dipole antenna. When the material is used to cover the loop antenna, it can be represented as $Z_m$ in parallel with $Z_l$, as shown in Fig. 7(b). $Z_a$ can thus be calculated as $Z_a = \frac{Z_l * Z_m}{Z_l + Z_m} + \frac{(\omega M)^2}{Z_d}$. Fig. 7(c) illustrates the equivalent circuit when the dipole antenna is cut and replaced with the gas-sensitive material and $Z_a = Z_l + \frac{(\omega M)^2}{Z_d + Z_m}$. When the material covers the dipole antenna, the equivalent circuit is shown in Fig. 7(d) and $Z_a$ is represented as $Z_a = Z_l + \frac{(\omega M)^2}{Z_d || Z_m}$.

We then perform simulations to understand the tag's impedance changes when the sensing material is placed under different methods. We first utilize Ansys HFSS (High-Frequency Structure Simulator) [20] to simulate $Z_l$ and $Z_d$, and calculate the change of antenna impedance. We then calculate the phase variations based on Eq. 2. The result is shown in Fig. 8(a) and we can see that the phase variation induced by method A is larger than other methods.

We further conduct an experiment to verify this. We fabricate four tags with the same basic structure and perform tag modifications using the four methods respectively. Then, we place these tags inside a sealed glass box and vary the concentration of $CO_2$ from 500 to 5000 $ppm$. For each tag, we measure the phase readings before and after flushing $CO_2$ into the box and calculate the phase changes. We set the distance between the tag and the reader antenna as 15 $cm$ to ensure the reader can read the tag. Fig. 8(b) shows the phase variations for the four methods. We can see that Method A achieves a larger phase variation, matching the simulation result. Therefore, *we choose the loop antenna part to place the sensing material in a cut-and-replace manner.*

Now we investigate where to place the sensing material in the loop antenna region. We change the cut locations and conduct experiments to study the impact. Fig. 9 plots the phase variations for different cut locations. We find an interesting observation, i.e., as the cut location gets closer to the tag chip, the variation becomes larger. When we place the sensing material at location A1, the largest phase change is achieved. To explain the rationale behind this phenomenon, we utilize the HFSS tool to simulate the current distribution inside the tag antenna. As shown in Fig. 10, we can see that the distribution is highly unbalanced: the current at the edge is much weaker than the current near the tag IC. Thus, we select a location near the tag IC to place the material. Note that when we cut the antenna very close to the IC, there is a risk of damaging the IC. Thus, we place the sensing material with a distance of 3-5 $mm$ to ensure the IC function is not affected.

*3.2.3 Improving the Working Range.* When the gas-sensitive material is embedded in the tag antenna, we find that the working range drops dramatically from a few meters to just 15 $cm$. Such a short distance hinders it from being used for large-scale deployment. Based on Eq. 3, we know that the working distance is primarily determined by the reflection coefficient $\Gamma$, the gain of tag antenna $G_{tag}$, and the reader transmission power $P_t$. Due to FCC regulations, the maximum power a commercial RFID reader can transmit is 32 $dBm$ which is a constant. To improve the working range, we need to minimize the reflection coefficient $\Gamma$ and enlarge the tag

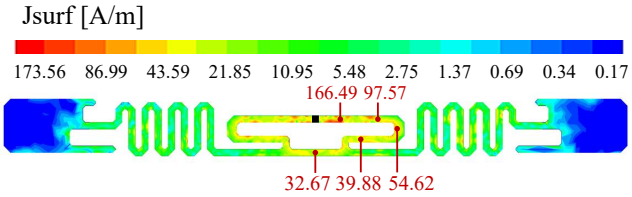


**Figure 10: Current distribution inside tag antenna.**

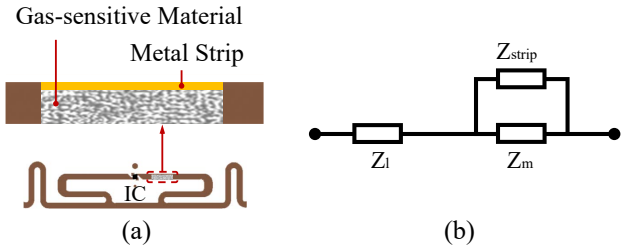


**Figure 11: Illustration of the loop antenna: (a) Enlarged view; (b) Equivalent circuit.**

antenna gain $G_{tag}$ after the gas-sensitive material is embedded in the tag.

**Minimizing** $\Gamma$**.** To minimize the reflection coefficient $\Gamma$, impedance matching needs to be achieved:

$$Z_a = Z_c^*, \tag{6}$$

where $Z_a$ and $Z_c$ are the impedance of the antenna and the impedance of the chip respectively. Traditional solutions for impedance matching are to fine-tune the parameters of the tag antenna [32]. However, directly applying such solutions is not suitable here. This is because the gas-sensitive material induces a large loss resistance, i.e., about 575 Ω (measured by Vector Network Analyzer) at the tag antenna. On the other hand, the resistance of the chip is only 30.53 Ω. Such a large gap makes fine-tuning parameters not working in our case.

To resolve this problem, inspired by the parallel resistance theory [28], which depicts that the overall resistance is mainly determined by the smaller resistance value, we propose a simple yet effective scheme to parallel a thin metal strip next to the gas-sensitive material, as shown in Fig. 11. Note that paralleling a metal strip to the material is not the same as Method B in Fig. 7.

To determine the design of the metal strip, we use a classical transmission line equivalent resistance model to model the resistance of such a structure [49]:

$$R = \frac{1}{\sigma}(\frac{l}{wh}), \tag{7}$$

where $l$ and $w$ are the length and width of the metal strip, and $h$ is the thickness of the metal strip, which is 10 $um$. Based on Eq. 7, we can optimize the width and length of the metal strip to achieve our desired resistance. We can then tune the other parameters of the tag to achieve impedance matching. For matching of imaginary part of the input and load impedance, we also tune the shape of the tag antenna.

**Table 1: The parameters of the Gastag.**

| Parameter | Value (mm) | Parameter | Value (mm) |
|---|---|---|---|
| R | 10.5 | D | 7.6 |
| P | 4.2 | Q | 3.2 |
| h | 21.1 | s | 12.2 |
| w | 6.9 | L | 60.4 |

**Increasing the Tag Antenna Gain** $G_{tag}$**.** Since the RFID tag is based on a folded dipole antenna and loop antenna, its gain is primarily related to the following parameters: the number of the fold, the width and height of the fold, the shape of the end load and loop antenna, and the material of the antenna [25], as shown in Fig. 13. We use the HFSS tool to conduct simulations to explore how these parameters affect the antenna's gain and the following conclusions are obtained. (i) Fig. 12(a) shows that *as the number of folds increases, the antenna gain decreases.* We thus select one fold for our sensing tag. (ii) Fig. 12(b) shows that *the wider the fold width, the larger the tag gain.* Fig. 12(c) shows that *a larger height of the fold leads to a larger tag gain.* Thus, we set a larger width and a larger height of the fold for our tag design. (iii) Fig. 12(d) and Fig. 12(e) show that *for the same area, circular shape achieves a larger gain.* Therefore, we design the shape of the end load and the loop antenna as circles. (iv) Fig. 12(f) shows that *the gain of a copper antenna is larger than that of an aluminum antenna.* We thus select copper as the antenna material. Tab. 1 summarizes the chosen antenna parameters based on the above observations. The simulation results in Fig. 14 show that the gain of the optimized tag is close to 2.2 $dB$ in the 902.75 - 927.25 $MHz$ band.

## 3.3 Tag Fabrication

In this section, we describe the fabrication process of the sensing tag. The workflow is shown in Fig. 15. It consists of four steps: (1) We first employ laser printing technology to shape the copper film according to the desired tag antenna design derived in Sec. 3.2; (2) Then, we use the conductive silver paste to embed the chip into the antenna and laminate the shaped copper film to the polyethylene terephthalate (PET) substrate [10]. The reason for selecting PET as the substrate is due to its stability, water resistance, flexibility, and low cost; (3) Next, we spray the gas-sensitive material evenly at the carefully chosen location on the substrate; (4) Finally, the whole structure is encapsulated with Biaxially Oriented Polypropylene (BOPP) [2], except the area where the sensing material is placed.

# 4 GAS SENSING

In this section, we introduce the method we developed to measure the gas concentration from the backscattered signal.

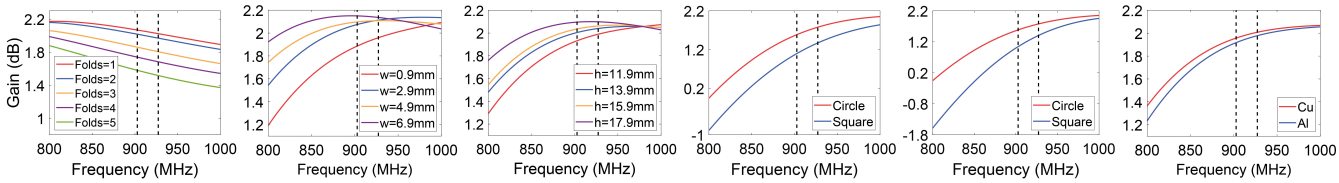


(a) Different numbers of fold (b) Different widths of the fold (c) Different heights of the fold (d) Different shapes of the load (e) Different loop antenna shapes (f) Different antenna materials

**Figure 12: Different parameters have different effects on the tag antenna gain.**

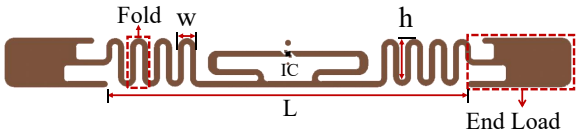


**Figure 13: Illustration of the basic tag parameters.**

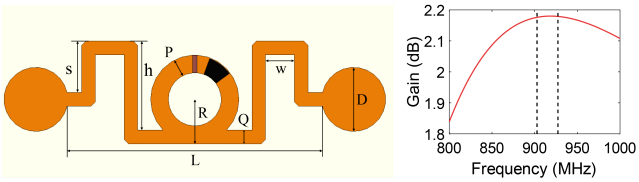


(a) Structure (b) Gain

**Figure 14: Optimized structure and gain of the designed tag antenna.**

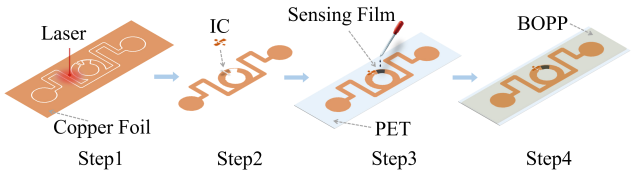


**Figure 15: Workflow of tag fabrication.**

## 4.1 Tag Sensing Model

We now extend the basic model, i.e., Eq.1 in Sec. 2 to accommodate the case when the gas concentration changes. Since the gas-sensitive material is embedded into the tag antenna, the tag's impedance $Z_a$ is a function of the gas concentration $\Lambda$. We thus can rewrite Eq.1 as follows:

$$\theta(\Lambda) = (\frac{2\pi}{\lambda} * 2d + \theta_{pol} + arg(-\frac{1}{Z_a(\Lambda) + Z_c(on)})) \bmod 2\pi. \quad (8)$$

From the above equation, we can see that the phase of the signal arriving at the reader is not only dependent on the tag antenna impedance, but also on tag-to-reader distance, and polarization match due to tag orientation. To further complicate matters, other factors such as human motion and multipath can also impact the phase of the received signal.

To tackle this problem, we adopt a twin-tag design to obtain the clean signal only affected by gas. Specifically, we deploy two tags next to each other, where one tag embeds a gas-sensitive material (sensing tag) and the other tag does not (reference tag). Since the reference tag and sensing tag

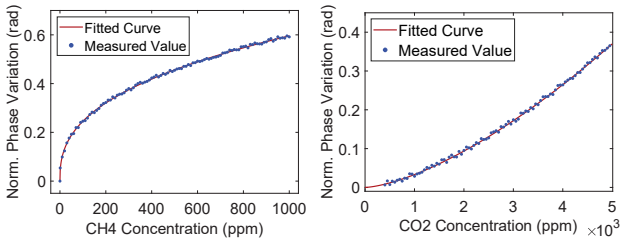


(a) $CH_4$ (b) $CO_2$

**Figure 16: Map phase reading to gas concentration.**

are close to each other, they experience almost the same environmental interference. The phase difference is as below:

$$\Delta\theta = \theta_s - \theta_r = arg(-\frac{1}{Z_a(\Lambda) + Z_c(on)}) - \theta_{tag,r}, \quad (9)$$

where $\theta_s$ and $\theta_r$ are the phases of the sensing tag and reference tag, respectively. We can see that $\Delta\theta$ is only related to the gas concentration.

## 4.2 Gas Concentration Sensing

Next, our goal is to model the relationship between the differential phase and gas concentration. We first calculate the phase difference between the two tags $[\Delta\theta_1, \Delta\theta_2, ..., \Delta\theta_I]$ at different gas concentration levels $[G_1, G_2, ..., G_I]$ in a hall environment. Then we normalize the data by subtracting the minimum phase difference. After that, we leverage polynomial curve fitting to find the best polynomial function $\Upsilon$ to minimize the difference between fitted values and ground-truth values:

$$\underset{n,p}{argmin}(|\Upsilon(n, p, \Delta\theta) - G|^2), \quad (10)$$

where $\Upsilon_i(n, p, \Delta\theta) = p_1\Delta\theta_i^n + p_2\Delta\theta_i^{n-1} + \cdots + p_n\Delta\theta_i + p_{n+1}$, $n$ and $p$ are the coefficients of the polynomial function, and $i$ the level index of gas concentrations.

We collect measurements for $CH_4$ and $CO_2$ in a sealed glass box by increasing the gas concentration gradually from 0 to 1000 $ppm$ at a step size of 10 $ppm$, and 500 to 5000 $ppm$ at a step size of 50 $ppm$, respectively. For each gas concentration, we collect 20 measurements. Note that this process is a one-time effort and the obtained model is environment independent. The ground truth gas concentration is obtained by using the gas Mass Flow Controller (MFC) [21]. We control the volume and speed of the gas to determine the gas

concentration and use it as the ground truth. Fig. 16 shows the results of the fitted curve. The dots in blue show phase variations for measured gas concentration, and the red line shows the fitted polynomial curve. By using the fitted curve, we can estimate gas concentration for a given phase variation value. For Impinj Speedway R420 RFID reader used in this work, the phase resolution is 0.0015 $rad$ [53].

To enable more accurate gas concentration sensing, we further leverage one observation: if we adopt signals of different frequencies, we obtain different amounts of phase variations under the same gas concentration change. Thus, we can exploit the frequency diversity of the RFID signals to boost the sensing performance. Specifically, we adopt the inherent frequency hopping mechanism of RFID to send CW signals of different frequencies. Note that we do not necessarily need to hop all the channels. We choose to hop five channels and adopt a weighted average scheme to obtain the final predicted concentration level $G_{final}$:

$$G_{final} = \frac{1}{F}\sum_{f=1}^{F} w_f \Upsilon(f), \tag{11}$$

where $f$ and $F$ are the channel number index and total number of channels. We assign weight to each channel based on the amount of phase variation obtained: $w_f = \frac{\Delta\theta(f)}{\sum_{i=1}^{F}\Delta\theta(i)}$. RFID reader hops to one new channel every 200 $ms$ [57]. Hopping to five channels in the test stage takes around one second, which is fast enough compared to the gas concentration changes that take minutes or even hours.

# 5 IMPLEMENTATION

**Hardware implementation.** We use an Impinj Speedway R420 reader [57] with a Larid S9028 directional antenna (9 $dBi$) as the transceiver. The reader operates in the frequency range of 902.75 – 927.25 $MHz$, and the transmission power is 32 $dBm$.

**Experiment setup.** For controlled experiments, we use MFC to adjust the gas concentration in a glass box (height: 30 $cm$, width: 30 $cm$, and length: 60 $cm$). Note that as $CO$ and $CH_4$ are toxic/hazardous, we only conduct uncontrolled experiments on $CO_2$. The ground-truth gas concentration is obtained using the gas MFC by controlling the volume and speed of the incoming gas. The maximum speed of the MFC is 10 $sccm$ (standard cubic centimeter per minute), and the accuracy is 0.01 $sccm$.

We conduct extensive experiments in three indoor environments, i.e., an open hall environment, an office, and an underground garage (UG), as shown in Fig. 17. In the *default setup*, we conduct experiments in the hall environment. We set the distance between the tag and reader antenna as 2.5 $m$. The spacing between two tags is 6 $cm$. We vary the concentrations of $CH_4$ and $CO_2$ in the glass box from 0 to 1000 $ppm$ at a step size of 10 $ppm$ and 500 to 5000 $ppm$ at a step size of 50 $ppm$. The concentration of $CO_2$ starts from 500 $ppm$ because the concentration of $CO_2$ in the air in our daily environment is around 400 $ppm$ [19]. Note that the gas-sensitive materials used for sensing $CH_4$ and $CO_2$ are rGO-PANI and rGO-CNT, respectively.

**Performance metric:** We use the absolute error between the estimated and the true gas concentration as the performance metric. The accuracy of commercial $CH_4$ sensors is around 10 $ppm$ [13] and the accuracy of commercial $CO_2$ sensors is 50 $ppm$ + 5% of reading [11].

# 6 EVALUATION

## 6.1 Performance of Gas Sensing Accuracy

**Accuracy in static scenarios.** We first study the accuracy of Gastag in static scenario. We adopt the default experiment setup. Fig. 18 presents the cumulative distribution function (CDF) of the sensing error. We can see that Gastag can achieve a median error of 6.7 $ppm$ and a 90% percentile error of 17.2 $ppm$ for $CH_4$. For $CO_2$, the median error is around 12.6 $ppm$, and the 90% percentile error is 45.5 $ppm$. The achieved accuracy outperforms a lot of commodity gas sensors on the market.

**Accuracy in different concentration intervals.** To examine the performance of Gastag in different gas concentration intervals, we divide the whole gas concentration range, i.e., 0 to 1000 $ppm$ for $CH_4$ and 500 to 5000 $ppm$ for $CO_2$ into 10 equal intervals. The experiment setup is the same as the default setup. Fig. 19 plots the average error in different intervals. We can see that as the gas concentration increases, the estimation error also becomes larger. A rough linear relationship can be observed which means the percentage error is roughly a constant.

**Comparison with dedicated sensors.** We now compare the performance of the proposed Gastag system with commodity gas sensors. We employ two commodity sensors for each gas. Specifically, $CH_4$ gas sensors include FORENSICS sensor ($355, Sensor-1) [13] and TopTes PT520A sensor ($33, Sensor-2) [45]. The first one is a catalytic combustion sensor that operates based on the principle of catalytic combustion of methane and oxygen in the air. The other is an electrochemical sensor that utilizes the electrochemical reaction between methane gas and the electrodes for concentration measurement. $CO_2$ sensors include Gain Express sensor ($163, Sensor-3) and Sefimir sensor ($46, Sensor-4). These two sensors are based on Non-Dispersive InfraRed (NDIR) technology. They monitor gas concentration by measuring the light intensity at a specific infrared wavelength. Fig. 20 plots the CDF of gas sensing errors. We can see that Gastag outperforms low-end commodity sensors, i.e., sensor-2 ($33) and sensor-4 ($46). The performance of Gastag is comparable


(a) Hall (b) Office (c) Underground Garage (d) NLoS

**Figure 17: Experiment setup in different environments.**

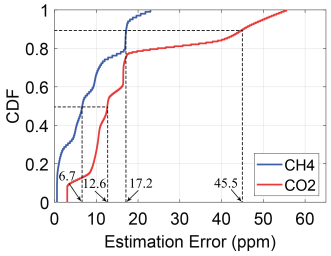


**Figure 18: CDF of estimation error for $CH_4$ and $CO_2$.**

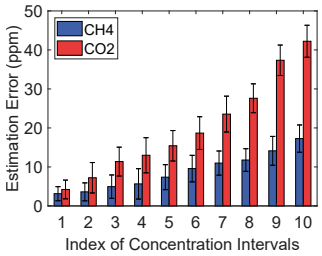


**Figure 19: Performance in different intervals.**

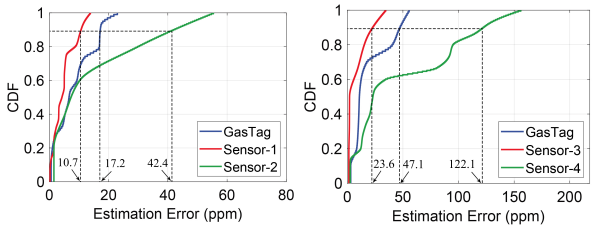


(a) $CH_4$ (b) $CO_2$

**Figure 20: Performance comparisons between Gastag and several commodity gas concentration sensors.**

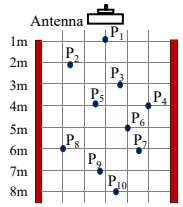


(a) Experiental Setup

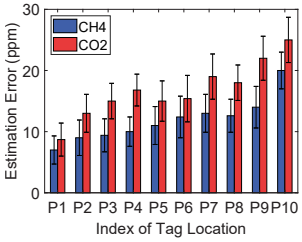


(b) Measurement Error

**Figure 21: Performance at different locations.**

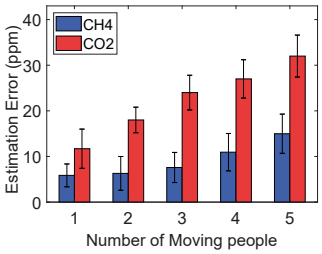


**Figure 22: Impact of human motion interference.**

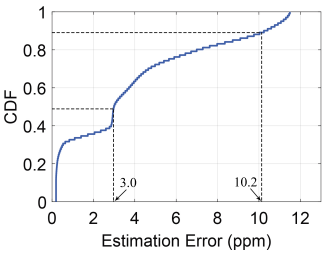


**Figure 23: CDF of concentration error for $CO$.**

to those high-end sensors, i.e., sensor-1 ($355) and sensor-3 ($163). Note that the cost of the tag is below 50 cents and one reader can cover many tags.

**Single-reader multi-location gas sensing.** One single RFID reader can work with multiple RFID tags deployed at different locations to monitor gas concentration. We deploy tags at 10 different locations as shown in Fig. 21(a) and use a single reader to collect RFID readings from the 10 twin-tags at the same time. Note that the reader is fixed at one location and does not move during the sensing process. The results are shown in Fig. 21(b). We can see that in general, when the tags are closer to the reader, lower error can be achieved. However, even for the tags located 8 $m$ away (i.e., $P_{10}$), our system can still achieve highly accurate sensing performance. This experiment also demonstrates the capability of simultaneously sensing gas concentrations at different locations with one single reader. The system latency for reading 20 tags is around one second. Note that gas concentration changes much more slowly, i.e., on the scale of minutes or even hours.

**Sensing performance in the presence of interference.** In a real environment, there exists interference (e.g., the human movements). To generate interference in the environment, we ask different numbers of persons to move around the sensing device. Fig. 22 shows the gas concentration estimation errors. We can clearly see that as the number of persons increases, the estimation error becomes larger. When there are 5 persons, the average estimation errors are still low, i.e., 12 $ppm$ and 32 $ppm$ for $CH_4$ and $CO_2$, respectively. This experiment demonstrates that the twin-tag design is effective in dealing with interference in the environment.

**Applying Gastag to sense other gases.** To examine the generalization capability of Gastag to sense other gases, we apply Gastag to sense another toxic gas $CO$. We synthesize Polypyrrole (PPy) and rGO to create a new material rGO-PPy.

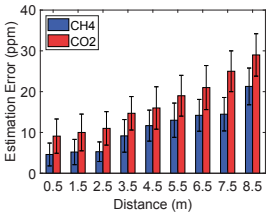


**Figure 24: Impact of tag-reader distance.**

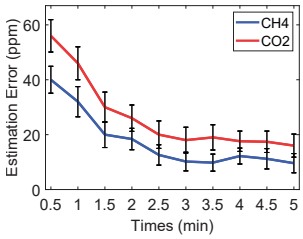


**Figure 25: Recovery time of the sensing material.**

We adopt the default setup for this experiment and change the concentration of $CO$ from 0 to 400 $ppm$ at a step size of 20 $ppm$. For each concentration, we collect 20 measurements. Fig. 23 shows that Gastag can achieve a median estimation error of 3 $ppm$ for $CO$ sensing, which demonstrates the generalization capability of Gastag to sense new gases.

## 6.2 Working Distance and Recovery Time

**Tag-reader distance.** In this experiment, we explore the maximum reader-tag working distance. We increase the distance at a step size of 0.5 $m$ and measure the gas concentration at each distance. We take the maximum distance we can still achieve a measurement error less than 30 $ppm$ as the maximum reader-tag working distance. The results are shown in Fig. 24. We can see that Gastag can still achieve an accurate sensing performance at a distance of 8.5 $m$. Note that directly replacing one antenna part with the sensing material results in a small working distance of 0.15 $m$. The working distance of the original RFID tag without the gas sensing function is around 6-8 $m$.

**The recovery time of the sensing material.** The recovery time of the sensing material is critical as it determines how often measurements can be made. In this experiment, we decrease the $CO_2$ concentration from 3000 $ppm$ to 500 $ppm$ very quickly (in a few seconds), and $CH_4$ concentration from 1000 $ppm$ to 0 $ppm$ very quickly. We then start measuring the concentration error every 30 $s$. When the measured error becomes stable, we record the timestamp to calculate the recovery time. The results are shown in Fig. 25. We can see that the recovery time is around 3 $min$ for a full recovery. Note that a full recovery takes a longer time. In real scenarios, after we measure a $CO_2$ concentration of 3000 $ppm$, it takes less than 3 $min$ for the material to perform the next measurement if the new concentration is 2000 $ppm$. The smaller the concentration difference between two adjacent measurements, the less time it takes for the material to be ready to make the next measurement. Note that when the concentration is quickly changed within a short period of time, the concentration is usually not evenly distributed and it takes time (e.g., tens of seconds) for the concentration to stabilize.

## 6.3 Performance under Different Parameters

**Performance in NLoS scenarios.** To evaluate the performance of Gastag in NLoS scenarios, we place different objects between the tag and the reader, including a bill board (320 $cm \times 240\ cm \times 12\ cm$) and a paperboard (80 $cm \times 55\ cm \times 2\ cm$). The experiment setup is shown in Fig. 17(d). The results are shown in Fig. 26, we can see that the sensing error slightly increases in NLoS scenarios with an average error below 11 $ppm$ for $CH_4$, and below 13 $ppm$ for $CO_2$. The slightly increased error is due to the decreased signal strength.

**Performance in different environments.** We conduct extensive experiments in three indoor environments including an office, an underground garage (UG), and a hall. The deployment setup is the same as that in the hall scenario depicted in Sec. 5. For each scenario, we measure the received signal under different gas concentrations. The results are shown in Fig. 27. We can see that Gastag can achieve an average accuracy of 5 $ppm$, 18 $ppm$, 17 $ppm$, and 11 $ppm$, 26 $ppm$, 25 $ppm$ for $CH_4$ and $CO_2$, respectively. These results demonstrate that Gastag performs well in environments with different amounts of multipath.

**Impact of reference tag position.** To investigate the impact of the reference tag's position, we vary the distance between the reference tag and the sensing tag from 2 to 10 $cm$ at a step size of 2 $cm$. Fig. 28 illustrates the estimation errors under different distances, from which we see that Gastag can achieve an estimation error below 5 $ppm$ and 15 $ppm$ for $CH_4$ and $CO_2$ when the distance is larger than 6 $cm$. When the distance is smaller than 6 $cm$, the estimation errors become large. We believe this is due to the coupling effect when the two tags are close to each other. We thus select 6 $cm$ as the default distance between the reference tag and sensing tag.

**Impact of tag orientation.** We now evaluate the performance of Gastag under different tag orientations. We move the glass box from 30° to 150° at a step size of 30° on a radius of 2.5 $m$. Fig. 29 plots the results. We observe a similar estimation error at different orientations for Gastag. The errors are below 10 $ppm$ and 16 $ppm$ under all tag orientations. This is because we adopt the twin-tag scheme so the polarization mismatch due to orientation difference can be canceled out. Therefore, Gastag is robust against tag orientation diversity.

**Impact of temperature and humidity.** We then evaluate the impact of temperature and humidity on the system performance. We discover that when the temperature reaches 50 °C, the system's accuracy decreases by 19% for $CH_4$ and 16% for $CO_2$ compared to the accuracy at room temperature (25 °C). Furthermore, when the humidity is 80%, the accuracy decreases by 11% for $CH_4$ and 8% for $CO_2$ compared to the accuracy at the humidity level of 20%. This is

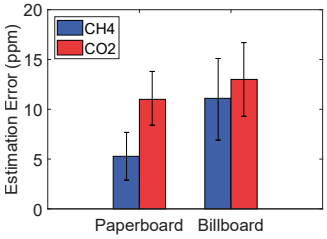


**Figure 26: Impact of NLoS blockages.**

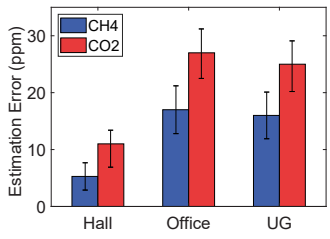


**Figure 27: Impact of different environments.**

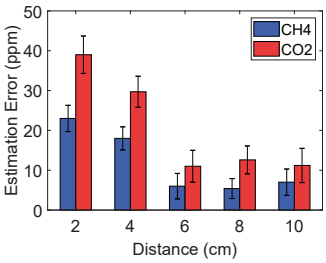


**Figure 28: Impact of reference tag position.**

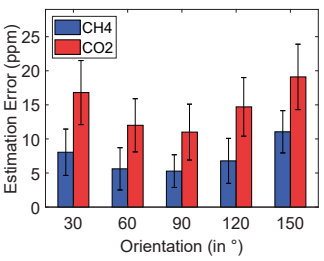


**Figure 29: Impact of tag orientation.**

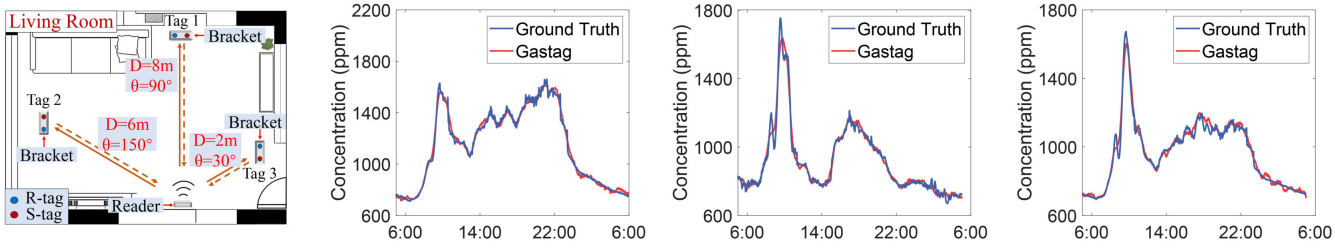


(a) Living Room (b) Tag 1 (c) Tag 2 (d) Tag 3

**Figure 30: Long-term real-time $CO_2$ monitoring.**

because high-humidity and high-temperature also affect the conductivity of the material which our system relies on for gas concentration sensing.

## 6.4 Case Study

In this case study, we aim to monitor the concentration fluctuation of $CO_2$ in an indoor environment over a long period of time. We deploy three pairs of tags at different locations in a living room. We also deploy commodity $CO_2$ sensors near the tag to collect measurements as baseline results. The detailed experiment setup is shown in Fig. 30(a). We monitor the concentration of $CO_2$ from 6 am of the first day to 6 am of the next day. The doors and windows are closed throughout the monitoring process. Fig. 30 shows the detailed concentration over time. We can see that the concentration values measured by the proposed system match those obtained from commodity gas sensors very well. We can further observe that: 1) Different locations exhibit different concentration fluctuations; 2) For most of the day, the $CO_2$ concentration in the room is above 1000 *ppm*, especially during morning and afternoon hours. These results demonstrate the necessity of monitoring the $CO_2$ concentration in home and office environments for the sake of our health.

# 7 RELATED WORK

Related work falls in the following three categories.

**Dedicated sensors for gas detection.** Many dedicated commercial sensors are available for gas sensing [9, 22, 38, 58]. The semiconductor sensors [38] utilize a semiconductor material that reacts with the target gas, causing a change in conductivity or resistance. The electrochemical sensors [58] utilize chemical reactions to generate an electrical output proportional to the gas concentration. Non-Dispersive Infrared (NDIR) sensors [9] detect gases by measuring the light intensity at a specific infrared wavelength. Photoionization detector (PID) sensors [22] use ultraviolet (UV) light to ionize gas molecules, generating a measurable current that indicates the gas concentration. However, most of these sensors require a power supply and are expensive. Consequently, when it comes to large-scale deployment, these sensors impose significant cost and maintenance burdens, making them unsuitable for long-term gas monitoring on a large scale. In contrast, Gastag uses cheap RFID tags as gas sensors to achieve performance comparable to commodity sensors.

**RF-based gas sensing.** A lot of effort has been devoted to using RF signals for gas sensing. For example, some early studies [24, 34, 36, 60] leverage terahertz signals to detect the presence and concentration of gases since many gas molecules absorb energy in the terahertz band. However, terahertz equipment typically costs at least tens of thousands of dollars [50]. Moreover, due to the high frequency, the sensing range of terahertz signal is about tens of centimeters [27]. In contrast, an RFID reader costs $600-1200 and the sensing range of RFID is a few meters. Another scheme [18] designs a dielectric resonator coated with a $TiO_2$ thin film as its sensing layer to sense gas in the millimeter-wave frequency band. However, this work only presents simulation results without conducting any real-life experiments.

Recently, some works have attempted to integrate sensing materials into RFID tags to sense different gases [16, 17, 26,

29, 30]. For example, Lee *et al.* [30] integrate gas-sensing material into the RFID tag antenna to detect $H_2$ gas. Ayesha *et al.* [16] utilize a vector network analyzer to measure the radar cross-section curve of tags for gas concentration sensing. However, the system performance is only evaluated at a single concentration level. In contrast, Gastag can measure the concentration of gases in a wide range. Ajith *et al.* [29] achieve coarse-grained gas sensing by measuring the minimum power required to make the tag readable which is related to the gas concentration. However, the process of measuring the minimum power through gradually increasing the transmission power is time consuming and troublesome. Moreover, the above systems only have a very short working distance, i.e., less than 1 $m$.

In conclusion, the previous works did not address the issue of small sensing distance. Furthermore, some approaches require dedicated devices such as a network analyzer as the receiver. In contrast, Gastag transforms the RFID tag into a gas sensor by quantifying the mathematical relationship between gas concentration and signal phase variation without compromising the tag-reader working distance. Moreover, Gastag uses commercial readers to perform gas sensing and achieves high sensing accuracy in a large concentration range. The working distance is significantly increased to 8.5 $m$, making large-scale deployment possible.

**RFID-based sensing.** RFID technology has been investigated in many sensing applications, e.g., localization [54, 56], activity and gesture recognition [12, 48], and target material identification [15, 55, 61]. For example, FaHo [62] uses radio frequency holograms to locate RFID tags. Grfid [64] performs accurate and robust gesture recognition by developing a weighted DTW method. RIO [43] employs tag coupling effect to sense touch gestures. Tagscan [55] and Tagtag [61] utilize tags to perform material recognition. Recently, some works have tried to utilize RFID tags to sense humidity and temperature [42, 44, 51, 52]. Radislav *et al.* [42] utilize a network analyzer to sense humidity with a sensing distance smaller than 50 $cm$ and the signal frequency is 13.56 $MHz$. Our work focuses on gas sensing which is more challenging and the achieved sensing distance (8.5 $m$) is orders of magnitude larger. Ju *et al.* [51] embed dedicated sensors (e.g., temperature sensors) in the tag, and the sensing capability of this system directly comes from the sensors employed. Our work turns the whole RFID tag as a gas sensor through quantifying the mathematical relationship between gas concentration and signal phase variation. Compared to these systems, gas sensing with wireless signals is more difficult. This is because the signal variation caused by gas concentration change is much smaller. Gastag thus combines material science and wireless sensing technology to achieve long-range fine-grained gas sensing for the first time.

# 8 DISCUSSION

**Cost and Scalability:** The cost of the proposed tag is around 50 cents. The relatively high cost of an RFID reader can be well amortized by simultaneously working with many tags (e.g., 10-20 tags). On the other hand, a typical $CO_2$/$CH_4$ commodity sensor costs around $100-500. To enhance the scalability, a single reader can be connected to multiple antennas to further increase the number of tags connected to the reader [53]. Moreover, by placing the reader on a moving robot, we can further expand the working range and enable large-scale deployment. A similar robot-based strategy has been widely adopted in libraries for scanning books [33]. While some low-cost air quality monitoring solutions [8] can be deployed at scale, the accuracy is not high and they usually only provide a warning when the gas concentration exceeds a specified threshold rather than providing fine-grained concentration measurements. Some of these sensors also require frequent calibration to achieve stable results [7].

**Durability and Maintenance:** The durability of gas-sensitive materials can be affected by high temperature and high humidity. Under the extreme conditions (i.e., a temperature of 50°C and an air humidity of 100%), the designed material can last for around 6 months and it can last much longer in normal conditions.

**Selectivity and Sensing Multiple Gases:** There is a trade-off between selectivity and sensing multiple gases with one material. Some materials can be used to sense multiple gases. However, this causes problems when we have no idea of the gas type. So it is preferred one material is only sensitive to one particular gas. As the tag cost is low, we can employ multiple tags, each targeting one particular gas.

# 9 CONCLUSION

In this paper, we present the design, implementation, and evaluation of Gastag. The key idea of Gastag is to replace a small part of the RFID tag antenna with carefully designed synthetic material to achieve accurate gas sensing in a large concentration range. Delicate tag antenna design is proposed to address the issue of sharp working distance drop. Through both theoretical analysis and experiment evaluation, we demonstrate the effectiveness of the proposed system in real-world settings.

# ACKNOWLEDGEMENTS

This work was supported by the National Natural Science Foundation of China under grant number 62272388, 62372374, and 62372372, the Shaanxi International Science and Technology Cooperation Program 2023-GHZD-06, 2024GH-ZDXM-50, and the Shaanxi Science and Technology Innovation Team Project 2024RS-CXTD-05. We would also like to thank Dr. Fuwei Wang and Zhouhu Deng for their help during the process of our system development.

## REFERENCES


[1] Jeffrey S Amthor. 2001. Effects of atmospheric CO2 concentration on wheat yield: review of results from experiments using various approaches to control CO2 concentration. *Field Crops Research* 73, 1 (2001), 1–34.

[2] AUDTMWH. 2020. https://a.co/d/3k2Katc/. (2020).

[3] Rahul Bhattacharyya, Christian Floerkemeier, and Sanjay Sarma. 2010. Low-cost, ubiquitous RFID-tag-antenna-based sensing. *Proc. IEEE* 98, 9 (2010), 1593–1600.

[4] Maria Cristina Caccami, Sabina Manzari, and Gaetano Marrocco. 2015. Phase-oriented sensing by means of loaded UHF RFID tags. *IEEE Transactions on Antennas and Propagation* 63, 10 (2015), 4512–4520.

[5] Varun Chandola, Arindam Banerjee, and Vipin Kumar. 2009. Anomaly detection: A survey. *ACM computing surveys (CSUR)* 41, 3 (2009), 1–58.

[6] Sung Hwan Cho, Jun Min Suh, Tae Hoon Eom, Taehoon Kim, and Ho Won Jang. 2021. Colorimetric sensors for toxic and hazardous gas detection: A review. *Electronic Materials Letters* 17 (2021), 1–17.

[7] H Chojer, PTBS Branco, FG Martins, MCM Alvim-Ferraz, and SIV Sousa. 2020. Development of low-cost indoor air quality monitoring devices: Recent advancements. *Science of The Total Environment* 727 (2020), 138385.

[8] Francesco Concas, Julien Mineraud, Eemil Lagerspetz, Samu Varjonen, Xiaoli Liu, Kai Puolamäki, Petteri Nurmi, and Sasu Tarkoma. 2021. Low-cost outdoor air quality monitoring and sensor calibration: A survey and critical analysis. *ACM Transactions on Sensor Networks (TOSN)* 17, 2 (2021), 1–44.

[9] Trieu-Vuong Dinh, In-Young Choi, Youn-Suk Son, and Jo-Chun Kim. 2016. A review on non-dispersive infrared gas sensors: Improvement of sensor detection limit and interference correction. *Sensors and Actuators B: Chemical* 231 (2016), 529–538.

[10] Duck. 2020. https://a.co/d/4LiJQRb/. (2020).

[11] Gain Express. 2020. https://a.co/d/inUwwIO/. (2020).

[12] Chao Feng, Jie Xiong, Liqiong Chang, Fuwei Wang, Ju Wang, and Dingyi Fang. 2021. Rf-identity: Non-intrusive person identification based on commodity rfid devices. *Proceedings of the ACM on Interactive, Mobile, Wearable and Ubiquitous Technologies* 5, 1 (2021), 1–23.

[13] FORENSICS. 2020. https://a.co/d/gq0Pre9/. (2020).

[14] Robin Gebbers and Viacheslav I Adamchuk. 2010. Precision agriculture and food security. *Science* 327, 5967 (2010), 828–831.

[15] Unsoo Ha, Junshan Leng, Alaa Khaddaj, and Fadel Adib. 2020. Food and liquid sensing in practical environments using {RFIDs}. In *17th USENIX Symposium on Networked Systems Design and Implementation (NSDI 20)*. 1083–1100.

[16] Ayesha Habib, Safia Akram, Mohamed R Ali, Taseer Muhammad, Sajeela Zainab, and Shafia Jehangir. 2023. Radio frequency identification temperature/CO2 sensor using carbon nanotubes. *Nanomaterials* 13, 2 (2023), 273.

[17] Fezza Haider, Shuo Liu, and George Shaker. 2018. Air quality monitoring using UWB radar. In *2018 18th International Symposium on Antenna Technology and Applied Electromagnetics (ANTEM)*. IEEE, 1–4.

[18] Hamida Hallil, Philippe Ménini, and Hervé Aubert. 2009. Novel millimeter-wave gas sensor using dielectric resonator with sensitive layer on TiO 2. In *SENSORS, 2009 IEEE*. IEEE, 226–228.

[19] James Hansen, Makiko Sato, Pushker Kharecha, David Beerling, Robert Berner, Valerie Masson-Delmotte, Mark Pagani, Maureen Raymo, Dana L Royer, and James C Zachos. 2008. Target atmospheric CO2: Where should humanity aim? *arXiv preprint arXiv:0804.1126* (2008).

[20] Ansys HFSS. 2020. https://www.ansys.com/products/electronics/ansys-hfss/. (2020).

[21] LD Hinkle and C Fl Mariano. 1991. Toward understanding the fundamental mechanisms and properties of the thermal mass flow controller. *Journal of Vacuum Science & Technology A: Vacuum, Surfaces, and Films* 9, 3 (1991), 2043–2047.

[22] PJ Hobbs, TH Misselbrook, and BF Pain. 1995. Assessment of odours from livestock wastes by a photoionization detector, an electronic nose, olfactometry and gas chromatography-mass spectrometry. *Journal of Agricultural Engineering Research* 60, 2 (1995), 137–144.

[23] Andy P Jones. 1999. Indoor air quality and health. *Atmospheric environment* 33, 28 (1999), 4535–4564.

[24] Yuichi Kado and Tadao Nagatsuma. 2009. Exploring SubTHz Waves for Communications, Imaging, and Gas Sensing. *Fog* 2, 02 (2009), 23–27.

[25] Nemai Chandra Karmakar. 2011. *Handbook of smart antennas for RFID systems*. John Wiley & Sons.

[26] Sung Gun Kim, Jaemoon Jun, Jun Seop Lee, and Jyongsik Jang. 2019. A highly sensitive wireless nitrogen dioxide gas sensor based on an organic conductive nanocomposite paste. *Journal of materials chemistry A* 7, 14 (2019), 8451–8459.

[27] Atsutse Kludze and Yasaman Ghasempour. 2023. {LeakyScatter}: A {Frequency-Agile} Directional Backscatter Network Above 100 {GHz}. In *20th USENIX Symposium on Networked Systems Design and Implementation (NSDI 23)*. 375–388.

[28] Kazuo Kurokawa. 2014. *An introduction to the theory of microwave circuits*. Elsevier.

[29] Ajith Adhur Kutty, Toni Björninen, Lauri Sydänheimo, and Leena Ukkonen. 2016. A novel carbon nanotube loaded passive UHF RFID sensor tag with built-in reference for wireless gas sensing. In *2016 IEEE MTT-S International Microwave Symposium (IMS)*. IEEE, 1–4.

[30] Jun Seop Lee, Jungkyun Oh, Jaemoon Jun, and Jyongsik Jang. 2015. Wireless hydrogen smart sensor based on Pt/graphene-immobilized radio-frequency identification tag. *ACS nano* 9, 8 (2015), 7783–7790.

[31] Curt Levis, Joel T Johnson, and Fernando L Teixeira. 2010. *Radiowave propagation: physics and applications*. John Wiley & Sons.

[32] Liyao Li, Yaxiong Xie, Jie Xiong, Ziyu Hou, Yingchun Zhang, Qing We, Fuwei Wang, Dingyi Fang, and Xiaojiang Chen. 2022. SmartLens: sensing eye activities using zero-power contact lens. In *Proceedings of the 28th Annual International Conference on Mobile Computing And Networking*. 473–486.

[33] Jia Liu, Feng Zhu, Yanyan Wang, Xia Wang, Qingfeng Pan, and Lijun Chen. 2017. RF-scanner: Shelf scanning with robot-assisted RFID systems. In *IEEE INFOCOM 2017-IEEE Conference on Computer Communications*. IEEE, 1–9.

[34] Xiaofei Lu, Nicholas Karpowicz, Yunqing Chen, and X-C Zhang. 2008. Systematic study of broadband terahertz gas sensor. *Applied Physics Letters* 93, 26 (2008).

[35] Micromeritics. 2020. https://www.micromeritics.com/asap-2460-2425/. (2020).

[36] Daniel M Mittleman, Rune Hylsberg Jacobsen, Ramesh Neelamani, Richard G Baraniuk, and Martin C Nuss. 1998. Gas sensing using terahertz time-domain spectroscopy. *Applied Physics B* 67, 3 (1998), 379–390.

[37] Azad Mohammed and Avin Abdullah. 2018. Scanning electron microscopy (SEM): A review. In *Proceedings of the 2018 International Conference on Hydraulics and Pneumatics—HERVEX, Băile Govora, Romania*, Vol. 2018. 7–9.

[38] S Roy Morrison. 1981. Semiconductor gas sensors. *Sensors and Actuators* 2 (1981), 329–341.

[39] Alexandru Oprea, Nicolae Bârsan, and Udo Weimar. 2009. Work function changes in gas sensitive materials: Fundamentals and applications. *Sensors and Actuators B: Chemical* 142, 2 (2009), 470–493.

[40] Hui Pan and Yuan Ping Feng. 2008. Semiconductor nanowires and nanotubes: Effects of size and surface-to-volume ratio. *ACS nano* 2, 11 (2008), 2410–2414.

[41] PIRG. 2022. pirg.org/resources/methane-gas-leaks/. (2022).

[42] Radislav A Potyrailo and Cheryl Surman. 2013. A passive radio-frequency identification (RFID) gas sensor with self-correction against fluctuations of ambient temperature. *Sensors and Actuators B: Chemical* 185 (2013), 587–593.

[43] Swadhin Pradhan, Eugene Chai, Karthikeyan Sundaresan, Lili Qiu, Mohammad Khojastepour, and Sampath Rangarajan. 2017. RIO: A Pervasive RFID-based Touch Gesture Interface. (2017), 261–274.

[44] Swadhin Pradhan and Lili Qiu. 2020. Rtsense: passive rfid based temperature sensing. In *Proceedings of the 18th Conference on Embedded Networked Sensor Systems*. 42–55.

[45] PT520A. 2020. https://a.co/d/6NEAVS3/. (2020).

[46] Xinming Qian, Ruoheng Zhang, Qi Zhang, Mengqi Yuan, and Yao Zhao. 2021. Cause analysis of the large-scale LPG explosion accident based on key investigation technology: a case study. *ACS omega* 6, 31 (2021), 20644–20656.

[47] V Ramya and B Palaniappan. 2012. Embedded system for Hazardous Gas detection and Alerting. *International Journal of Distributed and Parallel Systems (IJDPS)* 3, 3 (2012), 287–300.

[48] Longfei Shangguan, Zimu Zhou, and Kyle Jamieson. 2017. Enabling gesture-based interactions with objects. In *Proceedings of the 15th Annual International Conference on Mobile Systems, Applications, and Services*. 239–251.

[49] Martin R Stiglitz and Christine Blanchard. 1992. Transmission Line Design Handbook. *Microwave Journal* 35, 2 (1992), 184–185.

[50] Daniel J Tyree, Parker Huntington, Jennifer Holt, Ajani L Ross, Robert Schueler, Douglas T Petkie, Steve S Kim, Claude C Grigsby, Christopher Neese, and Ivan R Medvedev. 2022. Terahertz spectroscopic molecular sensor for rapid and highly specific quantitative analytical gas sensing. *ACS sensors* 7, 12 (2022), 3730–3740.

[51] Ju Wang, Omid Abari, and Srinivasan Keshav. 2018. Challenge: RFID hacking for fun and profit. In *Proceedings of the 24th Annual International Conference on Mobile Computing and Networking*. 461–470.

[52] Ju Wang, Liqiong Chang, Shourya Aggarwal, Omid Abari, and Srinivasan Keshav. 2020. Soil moisture sensing with commodity RFID systems. In *Proceedings of the 18th International Conference on Mobile Systems, Applications, and Services*. 273–285.

[53] Ju Wang, Jianyan Li, Mohammad Hossein Mazaheri, Keiko Katsuragawa, Daniel Vogel, and Omid Abari. 2020. Sensing finger input using an rfid transmission line. In *Proceedings of the 18th Conference on Embedded Networked Sensor Systems*. 531–543.

[54] Jue Wang, Deepak Vasisht, and Dina Katabi. 2014. RF-IDraw: Virtual touch screen in the air using RF signals. In *Acm Conference on Sigcomm*.

[55] Ju Wang, Jie Xiong, Xiaojiang Chen, Hongbo Jiang, Rajesh Krishna Balan, and Dingyi Fang. 2017. TagScan: Simultaneous target imaging and material identification with commodity RFID devices. In *Proceedings of the 23rd Annual International Conference on Mobile Computing and Networking*. 288–300.

[56] Ju Wang, Jie Xiong, Hongbo Jiang, Xiaojiang Chen, and Dingyi Fang. [n. d.]. D-Watch: Embracing Bad multipaths for device-free localization with COTS RFID devices. *IEEE/ACM Transactions on Networking (TON)* 25, 6 ([n. d.]), 3559–3572.

[57] Teng Wei and Xinyu Zhang. 2016. Gyro in the air: tracking 3d orientation of batteryless internet-of-things. In *Proceedings of the 22nd Annual International Conference on Mobile Computing and Networking*. 55–68.

[58] Werner Weppner. 1987. Solid-state electrochemical gas sensors. *Sensors and Actuators* 12, 2 (1987), 107–119.

[59] Zuquan Wu, Xiangdong Chen, Shibu Zhu, Zuowan Zhou, Yao Yao, Wei Quan, and Bin Liu. 2012. Room temperature methane sensor based on graphene nanosheets/polyaniline nanocomposite thin film. *IEEE Sensors Journal* 13, 2 (2012), 777–782.

[60] Yuanjiang Xiang, Jiaqi Zhu, Leiming Wu, Qi You, Banxian Ruan, and Xiaoyu Dai. 2017. Highly sensitive terahertz gas sensor based on surface plasmon resonance with graphene. *IEEE Photonics Journal* 10, 1 (2017), 1–7.

[61] Binbin Xie, Jie Xiong, Xiaojiang Chen, Eugene Chai, Liyao Li, Zhanyong Tang, and Dingyi Fang. 2019. Tagtag: material sensing with commodity rfid. In *Proceedings of the 17th conference on embedded networked sensor systems*. 338–350.

[62] Huatao Xu, Dong Wang, Run Zhao, and Qian Zhang. 2019. FaHo: deep learning enhanced holographic localization for RFID tags. In *Proceedings of the 17th Conference on Embedded Networked Sensor Systems*. 351–363.

[63] Zhien Zhang, Shu-Yuan Pan, Hao Li, Jianchao Cai, Abdul Ghani Olabi, Edward John Anthony, and Vasilije Manovic. 2020. Recent advances in carbon dioxide utilization. *Renewable and sustainable energy reviews* 125 (2020), 109799.

[64] Yongpan Zou, Xiao Jiang, Jinsong Han, Kaishun Wu, Li Yun, and Lionel M. Ni. 2017. GRfid: A Device-Free RFID-Based Gesture Recognition System. *IEEE Transactions on Mobile Computing* 16, 2 (2017), 381–393.